THE GERONTOLOGICAL SOCIETY OF AMERICA®

Journals of Gerontology: Biological Sciences
cite as: *J Gerontol A Biol Sci Med Sci*, 2017, Vol. 72, No. 3, 319–328
doi:10.1093/gerona/glw073
Advance Access publication April 30, 2016

OXFORD

Original Article

Aggregation of the Inflammatory S100A8 Precedes Aβ Plaque Formation in Transgenic APP Mice: Positive Feedback for S100A8 and Aβ Productions

Maria Lodeiro,[1] Elena Puerta,[1] Muhammad-Al-Mustafa Ismail,[1] Patricia Rodriguez-Rodriguez,[1] Annica Rönnbäck,[1] Alina Codita,[1] Cristina Parrado-Fernandez,[1] Silvia Maioli,[1] Francisco Gil-Bea,[1,2] Paula Merino-Serrais,[1] and Angel Cedazo-Minguez[1]

[1]Division of Neurogeriatrics, Department of Neurobiology, Care Sciences, and Society, Center for Alzheimer Research, Karolinska Institutet, Stockholm, Sweden. [2]Division of Neurosciences, Department of Cellular and Molecular Neuropharmacology, Center for Applied Medical Research (CIMA), University of Navarra, Pamplona, Spain.

Address correspondence to Associate Professor Ángel Cedazo-Mínguez, Division of Neurogeriatrics, Department of Neurobiology, Care Sciences, and Society, Center for Alzheimer Research, Karolinska Institutet, NOVUM, 5th floor, SE-14186 Stockholm, Sweden. Email: Angel.Cedazo-Minguez@ki.se

Received May 27, 2015; Accepted April 7, 2016

Decision Editor: Rafael de Cabo, PhD

Abstract

Inflammation plays an important role in Alzheimer's disease (AD) and other neurodegenerative disorders. Although chronic inflammation in later stages of AD is well described, little is known about the inflammatory processes in preclinical or early stages of the disease prior to plaque deposition. In this study, we report that the inflammatory mediator S100A8 is increased with aging in the mouse brain. It is observed as extracellular aggregates, which do not correspond to corpora amylacea. S100A8 aggregation is enhanced in the hippocampi of two different mouse models for amyloid-β (Aβ) overproduction (Tg2576 and TgAPParctic mice). S100A8 aggregates are seen prior the formation of Aβ plaques and do not colocalize. In vitro treatment of glial cells from primary cultures with $A\beta_{42}$ resulted in an increased production of S100A8. In parallel, treatment of a neuronal cell line with recombinant S100A8 protein resulted in enhanced $A\beta_{42}$ and decreased $A\beta_{40}$ production. Our results suggest that important inflammatory processes are occurring prior to Aβ deposition and the existence of a positive feedback between S100A8 and Aβ productions. The possible relevance of aging- or AD-dependent formation of S100A8 aggregates in the hippocampus thus affecting learning and memory processes is discussed.

Keywords: Alzheimer's disease—S100A8—Amyloid beta—Neuroinflammation—Corpora amylacea

Alzheimer's disease (AD) is a chronic progressive neurodegenerative disorder characterized by cognitive decline and is also the main cause of dementia (1). AD (reviewed in (2)) is histopathologically characterized by the presence of extracellular amyloid plaques and intraneuronal neurofibrillary tangles in the brain. The amyloid plaques consist of the beta amyloid peptide (Aβ) (3), which is formed by proteolytic cleavage of the amyloid precursor protein (APP) (4), whereas the neurofibrillary tangles are composed of aggregates of hyperphosphorylated tau protein (5).

Increasing evidence suggested that inflammatory processes play a significant role in the pathophysiology of AD (6). Several epidemiological studies reported that long-term use of nonsteroidal anti-inflammatory drugs (NSAIDs) substantially reduced AD risk (7–9). In other studies, however, the use of NSAIDs did not show beneficial effects on cognition in AD (10,11). Nevertheless, it is known that chronic brain inflammation is present in AD at advanced stages of the pathology when the presence of extracellular amyloid plaques is apparent (12). In these cases, an increase in activated astrocytes and microglia as well as in the expression of different proinflammatory molecules, such as interleukin-1 (IL-1) and tumor necrosis factor alpha (TNFα), within the brain is observed (6). Regarding the inflammatory events occurring at early stages of AD,

little is known, although the presence of inflammatory cytokines (IL-12 and interferon-γ) before the occurrence of amyloid plaques has been described in different mouse models relevant for AD (13,14). In a mouse model of AD, Ferretti and colleagues found an upregulation of key markers of inflammation such as iNOS, IL-1β, and COX2 along the intraneuronal accumulation of Aβ oligomeric species and proposed that early inflammatory processes are important events in the preplaque stages of amyloid pathology (15).

In AD brains several proinflammatory mediators are increased, including microglial infiltration and activation, and levels of several S100 calcium-binding proteins (S100B, S100A6, S100A9, and S100A12) (6). Apart from their involvement in AD, they also play a role in inflammatory and autoimmune diseases and many types of cancer (16). S100A8 is a ligand of receptor for advanced glycation endproduct (RAGE), a multiligand receptor in the immunoglobulin superfamily, which also binds other ligands including advanced glycation endproduct (AGE), the high-mobility group protein B1 (HMGB1), and Aβ (17,18). Interestingly, RAGE—which is expressed in microglia, neurons, and astrocytes (19,20)—mediates the transport of Aβ from the circulation across the blood–brain barrier and therefore plays a role in its accumulation into the brain (21). In addition to S100A8, RAGE binds monomeric and fibrillary forms of Aβ and β-sheet fibril structures (22,23), and its activation is involved in inflammatory responses, promoting synaptic dysfunction and neurodegeneration (24).

In the present study, we aimed to explore the associations between the inflammatory mediator S100A8 and Aβ productions in the brain. For this purpose, we have used two different mouse models of brain Aβ accumulation (Tg2576 and TgAPParctic) at two different ages or stages in the pathology (pre- and post-amyloid accumulation in brain). Tg2576 mice carry the Swedish double mutation, which causes an overproduction of Aβ in the brain and presents extracellular Aβ plaques around the age of 12 months (25). TgAPParc mice overexpress human APP with the arctic mutation, which alters the properties of Aβ, resulting in enhanced formation of protofibrils (26). In vitro, we used primary astrocyte cultures and a neuroblastoma cell line to study the possible interactions between Aβ and S100A8 productions. Our results are in agreement with the idea that significant inflammatory processes are occurring in the brain prior to Aβ deposition and with the existence of regulatory feedback loops between S100A8 and Aβ production.

Materials and Methods

Animals

Young (pre-Aβ plaques; 6- to 8-month-old) and old (post-Aβ plaques; 18- to 24-month-old) Tg2576 transgenic mice, overexpressing human amyloid precursor protein (hAPP) carrying the Swedish familial mutation (K670N/M671L) under the genetic mixed hybrid background C57BL/6/SJL, were used. Additionally, we used young (pre-Aβ plaques; 3-month-old) and old (post-Aβ plaques; 9-month-old) homozygous TgAPParc, overexpressing hAPP carrying the Arctic mutation (E693G) under the genetic mixed hybrid background C57BL/6/CBA. For comparison, respective wild-type (WT) littermates of the same age and genetic background were used.

All mice were kept under controlled conditions of humidity and temperature on a 12-hour light–dark cycle. Food and water were provided ad libitum. Animals were sacrificed by decapitation, and the brains were immediately frozen on dry ice and stored at −80°C. Experimental procedures were conducted in accordance with the European regulation and were approved by the ethical committee of Karolinska Institutet.

Cellular Culture and Treatments

Cerebellar tissue from 14-day-old Sprague–Dawley rat embryos was homogenized in Dulbecco's Modified Eagle Medium: Nutrient Mixture F-12 (DMEM-F12) with 10% fetal bovine serum and 2% B27 supplement (Life Technologies, Carlsbad, CA). Cultures used for the experiments contained on average 300,000 ± 10,000 cells per well. Most cells were flat, resembling inactivated astrocytes (27). Prior treatments, astrocytes were serum starved for 24 hours. Serum deprivation did not cause morphological changes in astrocytes, cells showing mostly round morphology with bright refringency and small dark nuclei (data not shown). $A\beta_{42}$ (Sigma-Aldrich, St. Louis, MO) was dissolved in serum-free minimum essential medium and incubated at 37°C with sporadic shaking for 24 hours to allow aggregation (28). Treatments with $A\beta_{42}$ were done at 0.5 μM for 24 hours. Ethical consent for experiments with primary cultures was received from the regional ethical committee of Karolinska Institutet.

Human SH-SY5Y neuroblastoma cells were obtained from the American Type Culture Collection and cultured in a 1:1 mixture of DMEM/F-12 supplemented with 10% fetal bovine serum in 75-cm^2 plastic culture flasks (Corning, Tewksbury, MA) at 37°C with 5% CO_2. For immunofluorescence, cells were seeded at 50% confluence in cover slips, and for polymerase chain reaction (PCR) analysis and Western blotting, confluent cells were used. In both cases, cells were treated with the S100A8 recombinant protein at final concentrations of 10, 50, or 200 ng/mL for 24 hours. In Western blotting, phorbol myristate acetate (PMA, 50 ng/mL) was used as positive controls for 2- and 24-hour treatments.

Western Immunoblotting

Secreted APP (sAPP) was determined as previously described (29). Cellular conditioned media was collected and centrifuged for 10 minutes at 12,000 rpm to remove nonadherent cells and cell debris. Samples were mixed with tricine loading buffer (0.16 M Tris-HCl pH 6.8, 4% sodium dodecyl sulfate (SDS), 20% glycerol, 0.01% bromophenol blue, 0.1 M dithiothreitol added fresh) and heated (95°C, 5 minutes), and the proteins were separated by SDS–polyacrylamide gel electrophoresis using 7.5% acrylamide gels and then transferred to a nitrocellulose membrane (Schleicher & Schuell, Dassel, Germany). After blocking for 1 hour using 5% (w/v) dried milk in Tris-buffered solution containing 0.1% Tween-20, the membranes were incubated with the primary antibody 6E10 (Senetek, Maryland Heights, MO) at 1:100 dilution in the same solution, followed by anti-mouse immunoglobulin G horseradish peroxidase at 1:5,000 dilution (GE Health Care, Little Chalfont, UK).

To determine protein levels of S100A8 and RAGE, cell lysate preparations were used, and proteins were quantified using the bicinchoninic acid assay protein assay kit (Pierce, Rockford, IL). Equal amounts of protein were separated using 10% acrylamide gel and transferred to a nitrocellulose membrane (Schleicher & Schuell). Incubations with primary antibodies (S100A8 1:500, Santa Cruz, Dallas, TX; RAGE 1:1000, AB3711, Abcam, Cambridge, UK) were performed overnight, followed by incubation with anti-rabbit or anti-mouse immunoglobulin G at 1:2,000 dilutions (GE Health Care, Uppsala, Sweden).

Immunoreactivity was detected by the ECL detection system (GE Health Care). The relative density of immunoreactive bands on Western blots was calculated from the optical density multiplied by the area of the selected band following acquisition of the blot image using the ImageJ 1.383 software (NIH, Bethesda, MA). As loading control for sAPP, Ponceau staining of the blots was performed and the total protein stained bands were used for normalization. As for the S100A8

and RAGE determinations, loading was normalized with actin (using antibodies from Sigma-Aldrich; 1:1000, overnight) or tubulin (using antibodies from Sigma-Aldrich; 1:1000, overnight) levels, respectively.

RNA Extraction and Real-time PCR

RNA extraction and real-time PCR were performed as previously described (30). Total RNA was extracted from frozen hippocampal tissue using the RNeasy lipid tissue mini kit from Qiagen (Palo Alto, CA) following the manufacturer's instructions. Real-time PCR amplification assay for gene target was performed with a total volume of 20 µL in each well containing 10 µL of PCR Master Mix (Life Technologies), 2 µL of cDNA corresponding to 10 ng of RNA, and 1 µL of each TaqMan Gene Expression Assays (for mice: S100A8 Mm00496696_g1, glyceraldehyde 3-phosphate dehydrogenase (GAPDH) catalogue number 4352932E; for rat: S100A8 Rn00587579_g1, GAPDH Rn01775763_g1; for human: APP Hs00169098_m1, GAPDH Hs02758991_g1) from Life Technologies.

Immunofluorescence

Immunohistochemistry was performed on coronal sections of fresh-frozen brains from the hippocampus of Tg2576, TgAPParc, and WT mice. The sections were postfixed in 4% cold paraformaldehyde in phosphate-buffered saline (PBS, 0.1 M, pH 7.4) for 15 minutes and subsequently washed three times with PBS. After fixation, single immunochemistry was performed. All the slices were pretreated to prevent vessels autofluorescence with 2% H_2O_2 for 30 minutes, they were then blocked for 1 hour in PBS with 0.25% Triton-X and 3% bovine serum albumin. The sections were incubated overnight with the primary antibody goat anti-S100A8 (1:100; Santa Cruz), mouse anti-glial fibrillary acidic protein (GFAP) (1:300; BD Biosciences, London, UK), and rabbit anti-Iba1 (1:500; Wako, Neuss, Germany) and then for 2 hours at room temperature with the secondary antibody Alexa fluor 594 or 488 donkey anti-goat (1:1000; Invitrogen, Carlsbad, CA), Alexa fluor 546 goat anti-mouse (1:1000; Invitrogen), and Alexa fluor 633 goat anti-rabbit (1:1000; Invitrogen). 4,6 diamino-2-phenylindole (DAPI; Sigma) was used to identify the nuclei of cell bodies. Finally, the sections were rinsed in PBS and mounted using the fluorescence mounting medium ProLong Gold Antifade Reagent (Invitrogen). The sections were thoroughly washed in PBS between different steps. For negative control, the primary antibody was omitted.

Confocal imaging was performed with a Zeiss LSM 510 META confocal laser scanning system. The fluorescence was recorded through separate channels with a 10× (NA 0.45) and 20× lens (NA 0.8).

Treatments were performed after 24 hours in serum-free media, then cells were prefixed with 2% paraformaldehyde for 2 minutes and fixed with 4% paraformaldehyde for 20 minutes. Afterwards, cells were washed three times with PBS. All cover slips were blocked for 30 minutes in PBS with 0.1% Triton-X and 1% bovine serum albumin. The primary antibodies used were goat anti-S100A8 (1:100; Santa Cruz), rabbit anti-$A\beta_{40}$ (1:100; (24)), and rabbit anti-$A\beta_{42}$ (1:100; (31)). The secondary antibodies used were Alexa fluor 594 donkey anti-goat (1:1000) and Alexa fluor 488 chicken anti-rabbit (1:1000), respectively. Cover slips were first incubated overnight with the primary antibodies and then for 30 minutes at room temperature with secondary antibodies and DAPI to identify the nuclei of cell bodies. Finally, the cover slips were rinsed in PBS and mounted as described earlier. The cover slips were thoroughly washed in PBS between different steps. The primary antibody was omitted as a negative control. Confocal imaging was performed with a Zeiss LSM 510 META confocal laser scanning system. The fluorescences of DAPI, Alexa 594, and Alexa 488 were recorded through separate channels with a 63× lens (numerical aperture [NA] 1.3). For $A\beta_{40}$ and $A\beta_{42}$ quantifications, Alexa 488 fluorescence was recorded with a Zeiss LSM 510 METAL confocal laser scanning system with 20× lens (NA 0.8). Representative pictures were recorded with 100× lens (NA 1.45). In in vivo studies, quantification of S100A8 aggregates was performed using ImageJ software. Confocal pictures were open in a single channel to visualize exclusively the S100A8 aggregates. Data were expressed as percentage (mean ± *SEM*) of area occupied by aggregates in relation with the total area of the picture. In in vitro studies, quantification of fluorescence intensity in individual cells was performed with ImageJ software. Values were expressed as mean ± *SEM*. Data were expressed in reference to the respective control values (arbitrary units = 1).

Cresyl Violet Staining

Fast-cresyl violet staining was done to visualize the granules found in the corpora amylacea in the same sections used for immunohistochemistry. In brief, after the image processing, the sections were stained for 10 minutes with cresyl violet solution. Following the staining, sections were dehydrated and cleared with xylene. Images were taken with an optical microscope (Nikon eclipse E800M) at 20× (NA 0.75) under bright field optics.

Thioflavin-S Staining

After anti-S100A8 staining, slices were unmounted and stained with Thioflavin-S to visualize the Aβ plaques in green (1% Thioflavin-S in PBS during 15 minutes). The tissue was dehydrated in an ethanol series for 5 minutes per step (100%, 70%, 50% ethanol and PBS), and the sections were washed in phosphate buffer and mounted with ProLong Gold Antifade Reagent.

Aβ Measurements

SDS-soluble and formic acid (FA)-soluble (guanidine-extracted) Aβ40 and Aβ42 levels were quantified in brain homogenates from mice as previously reported (32,33). Levels of Aβ were expressed as fmol/µg protein. In SH-SY5Y cell extracts, total $A\beta_{40}$ and $A\beta_{42}$ were determined using commercial colorimetric enzyme-linked immunosorbent assay (ELISA) kits (Human $A\beta_{40}$ and $A\beta_{42}$, Wako) following the manufacturer's protocol. Aβ values were expressed as mean ± *SEM* in reference to the respective control values (arbitrary units = 1).

Cell Viability Assay

The Resazurin (Sigma) reagent was prepared in DMEM/F-12 at a final concentration of 20 µg/mL. SH-SY5Y cells were seeded in 24-well plates at 15 × 104 cells/well. After treatment with S100A8 (200 ng/mL; 24 hours), the plates were washed once in 1× PBS and incubated in a 400 µL working solution of Resazurin for 2 hours at 37°C. Fluorometric Resazurin reduction was measured in a Tecan plate reader, and the values were calculated by Magellan Data Analysis Software. Results were expressed as percentages compared with controls (untreated cells).

Statistical Analysis

Analyses of differences between two groups were carried out using the Mann–Whitney *U* test. In the analysis of S100A8 immunofluorescence, statistical comparisons between groups were made by analysis of variance followed by Bonferroni's multiple comparison post hoc test. Differences in $A\beta_{40}$ and $A\beta_{42}$ levels from the ELISA measurements were evaluated with a one-way analysis of variance followed by a Tukey's post hoc test. A p value less than .05 was considered significant.

Results

S100A8 Expression Is Increased in the Hippocampus of Tg2576 and TgAPParc Mice

We analyzed the pattern of S100A8 immunoreactivity in the hippocampus of Tg2576 and TgAPParc mice at two different ages representing preplaque stage (young) and Aβ plaques stage (old), respectively. As controls, we used WT littermates at the corresponding age.

The Tg2576 model presents extracellular Aβ plaques around the age of 12 months, showing high astrogliosis, dystrophic neurites, and cognitive impairment by this age (25). Results in Figure 1A

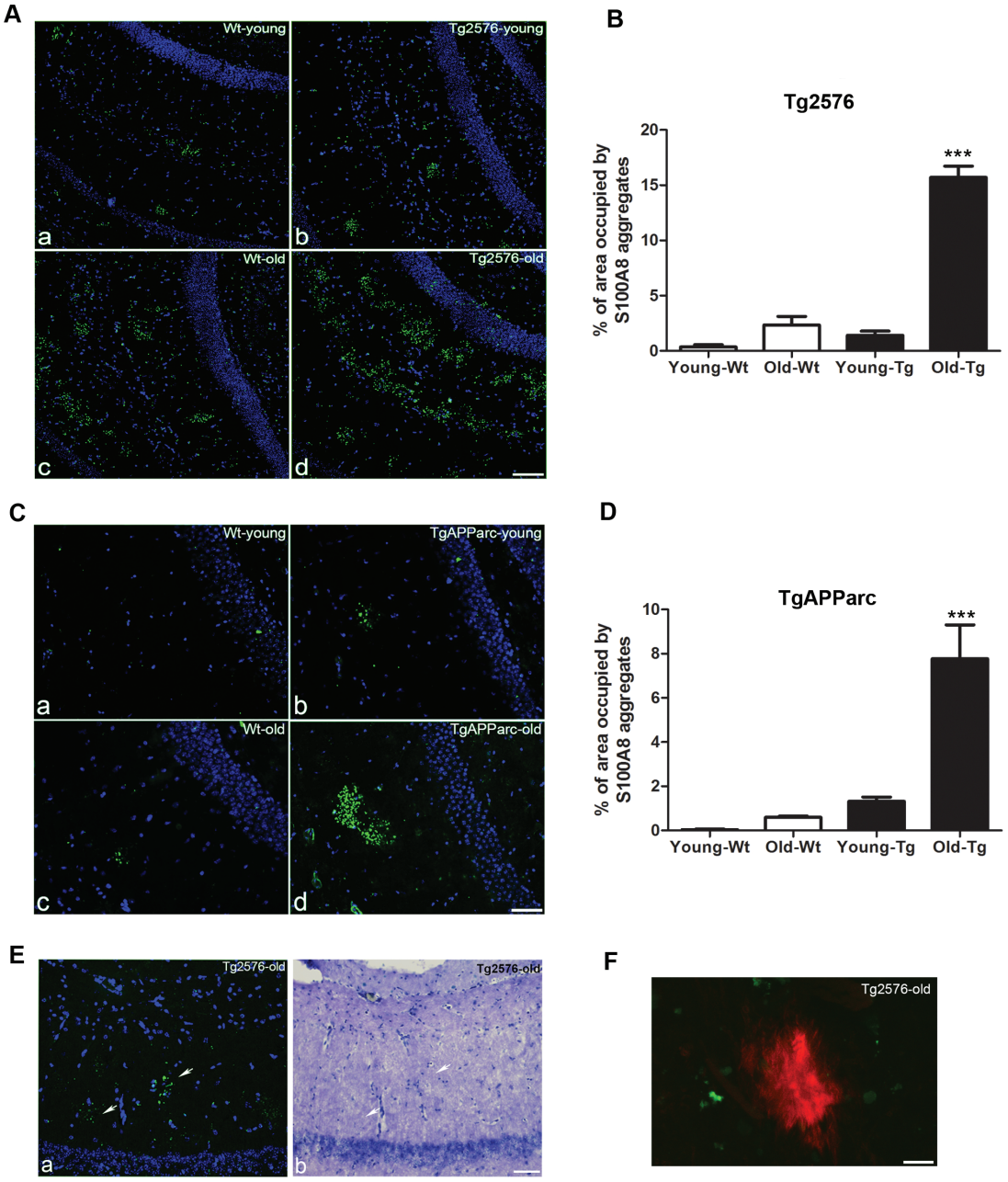

Figure 1. S100A8 aggregates are seen prior to Aβ plaque formation in transgenic APP mice. (**A**) Confocal microscopy of sections stained with anti-S100A8 (green) and 4,6 diamino-2-phenylindole (DAPI; blue) from the same field in the CA1 hippocampal region from wild-type (WT) and Tg2576 mice at two ages: young (8-month-old; upper panel (a), (b)) and old (18-month-old; lower panel (c), (d)). Scale bar 120 μm. (**B**) Quantification of S100A8 immunofluorescence in the brains of Tg2576 mice. (**C**) Confocal microscopy of sections stained with anti-S100A8 (green) and DAPI (blue) from the same field in the CA1 hippocampal region from WT and TgAPParc mice at two ages: young (3-month-old; upper panel (a), (b)) and old (9-month-old; lower panel (c), (d)). Scale bar 120 μm. (**D**) Quantification of S100A8 immunofluorescence in the brains of TgAPParc mice. (**E**) Representative image (a) from one of the sections in (A) stained with cresyl violet (b) showing with an arrow the S100A8 aggregates. Scale bar in (b): 100 μm. (**F**) Confocal microscopy image of a section from old Tg2576 mouse stained with Thioflavin-S to visualize the Aβ plaques (red) and S100A8 (green). Scale bar 20 μm. Both (B) Tg2576 and (D) TgAPParc mice show significant increases in S100A8 immunofluorescence with time ($p = .0001$ for Tg2576 and $p = .0003$ for TgAPParc compared with their respective WT littermates; analysis of variance with Bonferroni's multiple comparison test; mice $n = 3$ per group, three sections per mice).

show an increase in S100A8 immunoreactivity in the hippocampus of Tg2576 mice compared with their WT littermates. This happened at both preplaque (compare (a) vs (b)) and Aβ plaque stages (compare (c) vs (d)), the increase becoming more pronounced as the mice aged (Figure 1A, inset (d)). Aging also induced S100A8 accumulation in the hippocampus of WT mice (compare (a) vs (c)).

The young TgAPParc mouse shows intracellular Aβ accumulation and diffuse amyloid deposits in subiculum (at 4 months of age) which is followed by a characteristic spatiotemporal Aβ accumulation in interconnected brain regions; retrosplenial granular cortex at 6 months of age, thalamus at 9 months of age, and entorhinal cortex and the CA1 region of the hippocampus at 12–15 months of age (32). Similar to the Tg2576, TgAPParc mice revealed an increase in the immunoreactivity of S100A8 in the hippocampus compared with their WT littermates (Figure 1C, compare (a,c) vs (b,d)), being more pronounced at old ages.

Quantification of S100A8 immunofluorescence in WT, Tg2576, and TgAPParc animals is shown in Figure 1B and D, respectively. Both Tg2576 (Figure 1B) and TgAPParc mice (Figure 1D) show significant increases in S100A8 immunofluorescence with time compared with their respective WT littermates. In both mice models, accumulated S100A8 appears as extracellular granular aggregates in the *stratum oriens* and *stratum radiatum* of the hippocampus, areas of great importance for learning and memory processes. We checked whether the observed S100A8 aggregates were part of the *corpora amylacea* (CA) by staining the same sections with cresyl violet (34). Other members of the S100 family protein were reported to be part of CA (35), however, this was not the case for S100A8. For example, Figure 1E shows S100A8 staining (left) and cresyl violet staining (right) in a sample of Tg2576 old mice.

The same sections from the immunohistochemical analyses were also stained with Thioflavin-S in Tg2576 old animals to interrogate whether S100A8 aggregates localize with Aβ plaques. As seen in Figure 1F, no colocalization was found. Real-time PCR of hippocampal samples from old animals was performed to observe if the enhanced S100A8 immunoreactivity seen in TgAPP models was paralleled with increase in expression levels. As seen in Figure 2A, S100A8 mRNA expression was significantly enhanced in both Tg2576 and TgAPParc compared with their respective WT littermates (p = .028 and p = .015, respectively, n = 3–5). Analysis of cortical extracts from the same animals revealed that Tg2576 mice accumulated higher levels of both SDS-soluble and FA-soluble forms of $A\beta_{40}$ (Figure 2B) and $A\beta_{42}$ (Figure 2C) than TgAPParc mice. Figure 2D shows the $A\beta_{42}/A\beta_{40}$ ratio for each SDS-soluble and FA-soluble forms for both animal models.

As seen in Figure 3, S100A8 immunofluorescence was mainly extracellular, although some colocalization was found with glial markers, of which 98%–99% was with the astroglial marker GFAP and 1%–2% with the microglial marker IBA1. Moreover, the extracellular accumulation of S100A8 in Tg2576 and TgAPParc mice was confirmed because apparent areas of S100A8 in the brain of these animals did not colocalize with any cellular marker (GFAP, IBA1, and DAPI; arrows in Figure 3)

Positive Feedback Between $A\beta_{42}$ and S100A8 Productions In Vitro

To explore the existence of an association between the expressions of Aβ, S100A8, and their common receptor RAGE, we performed a series of in vitro experiments using recombinant $A\beta_{42}$ and S100A8.

We could not detect any expression of S100A8 in neurons from rat primary cultures or in human SH-SY5Y neuroblastoma cells in either basic conditions or after treatment with $A\beta_{42}$ (0.5 μM,

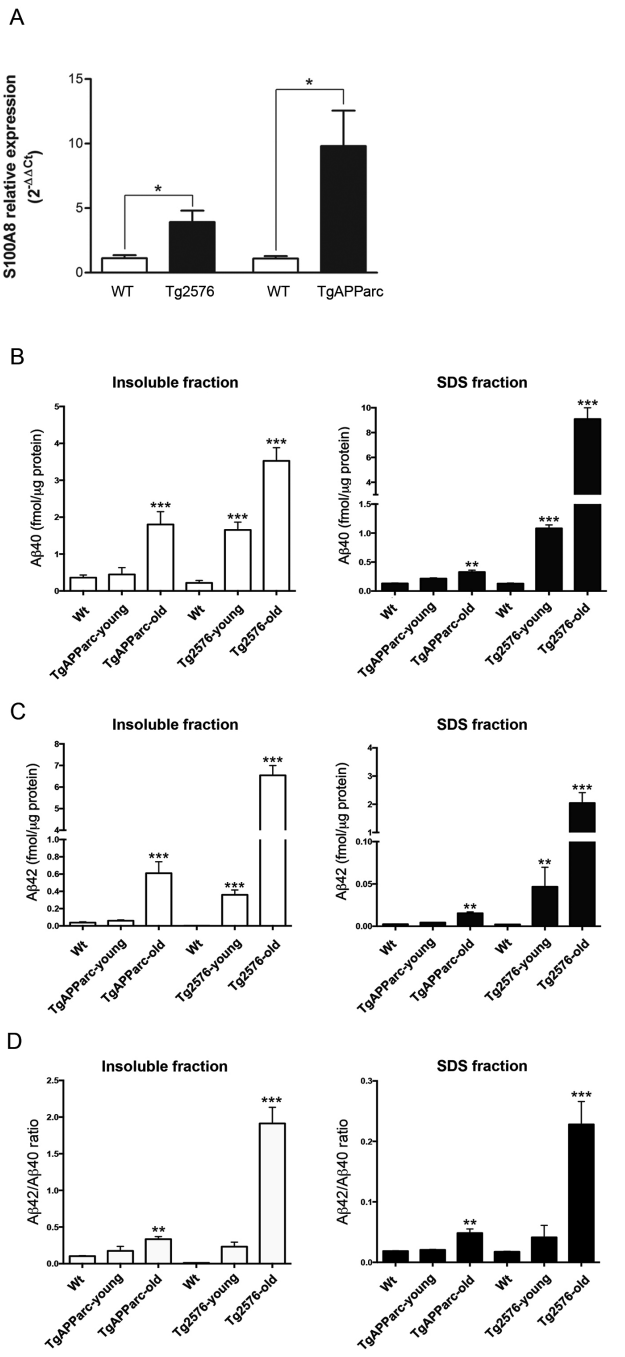

Figure 2. S100A8 expression and Aβ levels in transgenic APP mice. (**A**) S100A8 mRNA levels in the hippocampus of old Tg2576 and TgAPParc mice compared with their respective wild-type (WT) littermates. *p < .05; n = 4; Mann–Whitney U test. Enzyme-linked immunosorbent assay measurements of (**B**) $A\beta_{40}$ and (**C**) $A\beta_{42}$ in sodium dodecyl sulfate (SDS)-soluble (black bars) and insoluble (white bars) brain extracts from homozygous Tg2575 and TgAPParc mice (n = 3–5 per group). $A\beta_{40}$ and $A\beta_{42}$ levels in the respective WT animals did not differ significantly and were thus pooled for the analysis. (**D**) $A\beta_{42}/A\beta_{40}$ ratios in insoluble and SDS fractions, calculated from data shown in (C) and (B). All data are represented as mean values ± *SEM*. *p < .05; **p < .01; ***p < .001, analysis of variance followed by Tukey's post hoc test.

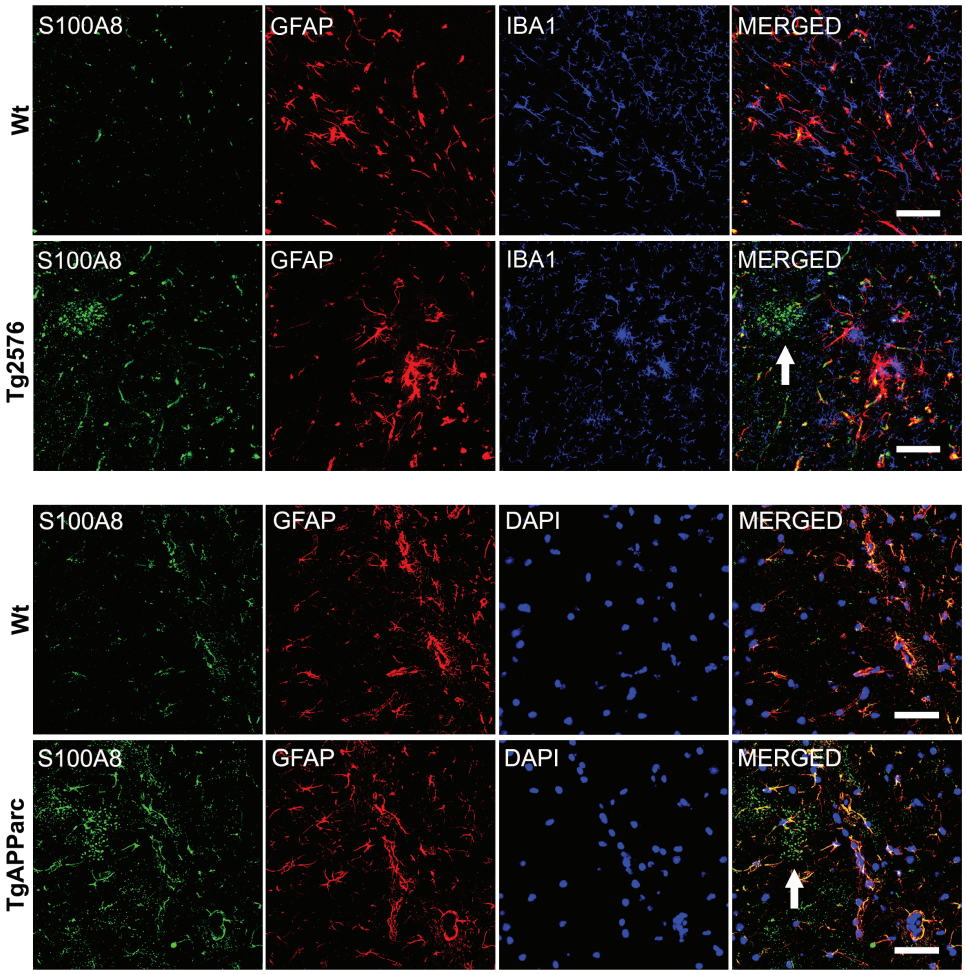

Figure 3. Brain aggregates of S100A8 are localized extracellularly. Upper panel: Confocal microscopy of sections stained with anti-S100A8 (green), GFAP (red), IBA1 (blue), and merged from the same field in the CA1 hippocampal region from wild-type (WT) and Tg2576 mice at 18 months of age. Lower panel: Confocal microscopy of sections stained with anti-S100A8 (green), GFAP (red), 4,6 diamino-2-phenylindole (DAPI; blue), and merged from the same field in the CA1 hippocampal region from WT and TgAPParc mice at 9 months of age. Scale bar 120 μm.

24 hours; data not shown). In rat primary astrocytes, $A\beta_{42}$ treatment (0.5 M, 24 hours) induced a statistically significant increase in S100A8 mRNA levels ($p < .001$; Figure 4A). Inmunocytochemical studies with confocal images analysis and immunoblotting studies corroborated a significant increase of S100A8 in astrocytes after treatment with $A\beta_{42}$ (Figure 4B and C, respectively). As seen in Figure 4C, S100A8 Western blot immunoreactivity was found at approximately 20–24 kDa, which would correspond to dimeric formations of the protein (36). In our paradigm, no signal was found at the expected molecular weight of 10 kDa (monomeric S100A8). The histograms in Figure 4B and C show the quantification of S100A8 protein in $A\beta_{42}$-treated (0.5 μM, 24 hours) versus untreated cells. In contrast, $A\beta_{42}$ treatment (0.5 μM, 24 hours) did not alter RAGE mRNA ($p = .7$; Figure 4D) nor protein levels in SH-SY5Y cells ($p = .5$; Figure 4E). Similarly, S100A8 treatment (200 mg/mL; 24 hours) did not affect RAGE expression in SH-SY5Y (data not shown).

On the other hand, treatment of human SH-SY5Y neuroblastoma cells with recombinant S100A8 (200 ng/mL; 24 hours) resulted in a significant increase of $A\beta_{42}$ production, and a parallel decrease in $A\beta_{40}$ production, as determined by ELISA. Thus, the $A\beta_{42}/A\beta_{40}$ ratio was significantly increased (Figure 5A). Imunocytochemical analysis using variant concentrations of S100A8 (10, 50, and 200 ng/mL; 24 hours) confirmed a marked S100A8-induced increase in $A\beta_{42}$ production. S100A8 treatment did not result in significant changes in $A\beta_{40}$ immunoreactivity (Figure 5B and C), although the highest concentration (200 ng/mL) showed a tendency toward reduced $A\beta_{40}$ ($p = .07$).

We next explored whether the S100A8-mediated $A\beta_{42}$ enhancement resulted from modifications in APP processing. As seen in Figure 5D, S100A8 (200 ng/mL; 24 hours) treatment did not modify the mRNA expression of APP ($p = .79$). We immunoblotted with the 6E10 antibody to analyze levels of α-secretase processed APP (sAPPα) in conditioned media from SH-SY5Y cells treated with S100A8 and from untreated cells (37). PMA was used as a positive control, as it is known that phorbolesters activate α-secretases, resulting in increased sAPPα levels in conditioned media (29). 6E10 immunoblotting revealed the presence of two bands with molecular masses of 90 and 120 kDa, corresponding to possible alternatively glycosylated forms of sAPPα (Figure 5E) (37). The densitometry of both bands was used for quantification. Resulting data were normalized against a loading control (total protein Ponceau staining of each band). Immunoreactivity data, expressed as percentage of sAPPα secretion in untreated cells, are shown in Figure 5F. PMA treatment

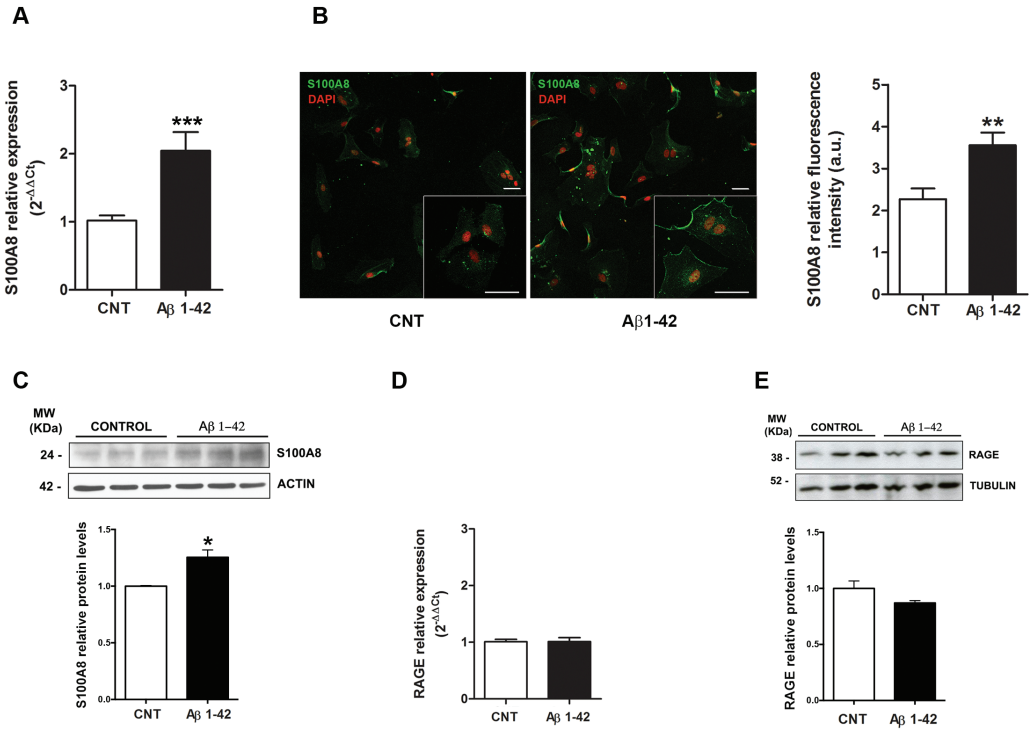

Figure 4. Effects of $A\beta_{42}$ (0.5 μM, 24 hours) on S100A8 and RAGE expressions. (**A**) S100A8 mRNA levels in astrocyte primary cultures treated with $A\beta_{42}$. (**B**) Confocal microscopy of astrocytes untreated (left panel) or treated (right panel) with $A\beta_{42}$ and stained with anti-S100A8 (green) and 4,6 diamino-2-phenylindole (DAPI; red). Scale bar 50 μm. Histogram in (B) shows means ± *SEM* from individual cell fluorescence intensity measures taken as arbitrary units (a.u). $^{**}p < .01$; $n = 5$ with a minimum of 10 cells measured per image and condition. (**C**) $A\beta_{42}$ increased S100A8 protein levels. $A\beta_{42}$ did not alter (**D**) RAGE mRNA nor (**E**) protein expression in SH-SY5Y cells. $^{*}p < .05$; $^{***}p < .001$; Mann–Whitney *U* test ($n = 3$–5, with experiments performed in triplicate).

induced significant changes in sAPPα (approximately 200%–400% of control values, both at 2 and 24 hours of treatment, $p = .001$). The effects of S100A8 treatment were apparent at 24 hours, resulting in a decrease in sAPPα production to approximately 60% of control values ($p = .028$, $n = 4$; Figure 5E and F).

Treatment with recombinant S100A8 (200 ng/mL; 24 hours) did not modify the viability of human SH-SY5Y cells as seen by the Resazurin cell viability assay (100 ± 3.2 in controls vs 99.15 ± 3.0 in S100A8-treated cells, $n = 9$).

Discussion

The molecular mechanisms leading to AD pathology are complex and have been shown to include dysfunctions in several biological processes such as protein (mis)folding, mitochondrial function, oxidative stress, inflammatory responses, or neurotransmission (38). The disease complexity is underlined by the existence of numerous genetic and environmental risk factors contributing to the AD pathogenesis (39). Increased Aβ load in the brain is considered one of the key characteristics of the disease pathology (39), although the pathological mechanisms of the Aβ cascade are not completely understood. Insoluble aggregates of the Aβ protein in various forms (from oligomers to fibrils) are strong candidates for initiating an inflammatory response in AD (39). Gliosis is seen in AD whereas activated astrocytes and microglia are characteristically found in abundance near neurons and plaques (6). An increased release of numerous pro-inflammatory cytokines (IL-1, TGF, and IL-6) and some S100 proteins have also been described in AD and in AD preclinical models (40). Regarding S100A8, a previous report showed a twofold increase of S100A8 mRNA levels in hippocampus from AD patients compared with nondemented controls (41). Kummer and colleagues demonstrated that deficiency in S100A9 improves Aβ burden in glial cells both in vitro and in vivo and that the heterodimer S100A8/S100A9 is upregulated in microglial cells surrounding the amyloid plaques in the APP/PS1 mouse model (42).

In the present article, we show that S100A8 is accumulated and forms nonfibrillar aggregates in the hippocampi of two different animal models, Tg2576 and TgAPParc, based on overexpression of APP with disease-causing mutations. Although with limitations (43), TgAPP animal models constitute a tool to investigate the effects resulting from Aβ accumulation in the brain, such as inflammatory responses or synaptic and cognitive dysfunction (25). Tg2576 mouse presents extracellular Aβ plaques around the age of 12 months (25). On the other hand, the TgAPParc mouse due to the characteristics of the Arctic mutation results in intracellular Aβ accumulation and enhanced formation of protofibrils (26,32). In both models, S100A8 aggregates are seen prior to Aβ plaques deposition.

S100A8 aggregates were also seen in WT mice as a result of aging, but to a lesser extent and much later than in both TgAPP mice models. Some members of S100 protein family are found in CA, an assemblage of granular structures characteristic of normal aged brain (35). CA also accumulates in AD (44), other neurodegenerative disorders, and cancer (45,46) and has been described to contain hexoses and other proteins, such as AGEs, heat shock proteins, Tau, and APP. Our results suggest that hippocampal S100A8 aggregates are outside CA, because they did not colocalize with the CA marker in cresyl violet staining. Moreover, in TgAPP mice, S100A8 aggregates were not seen in direct association with Aβ fibrillar plaques, as they did not stain with Thioflavin-S.

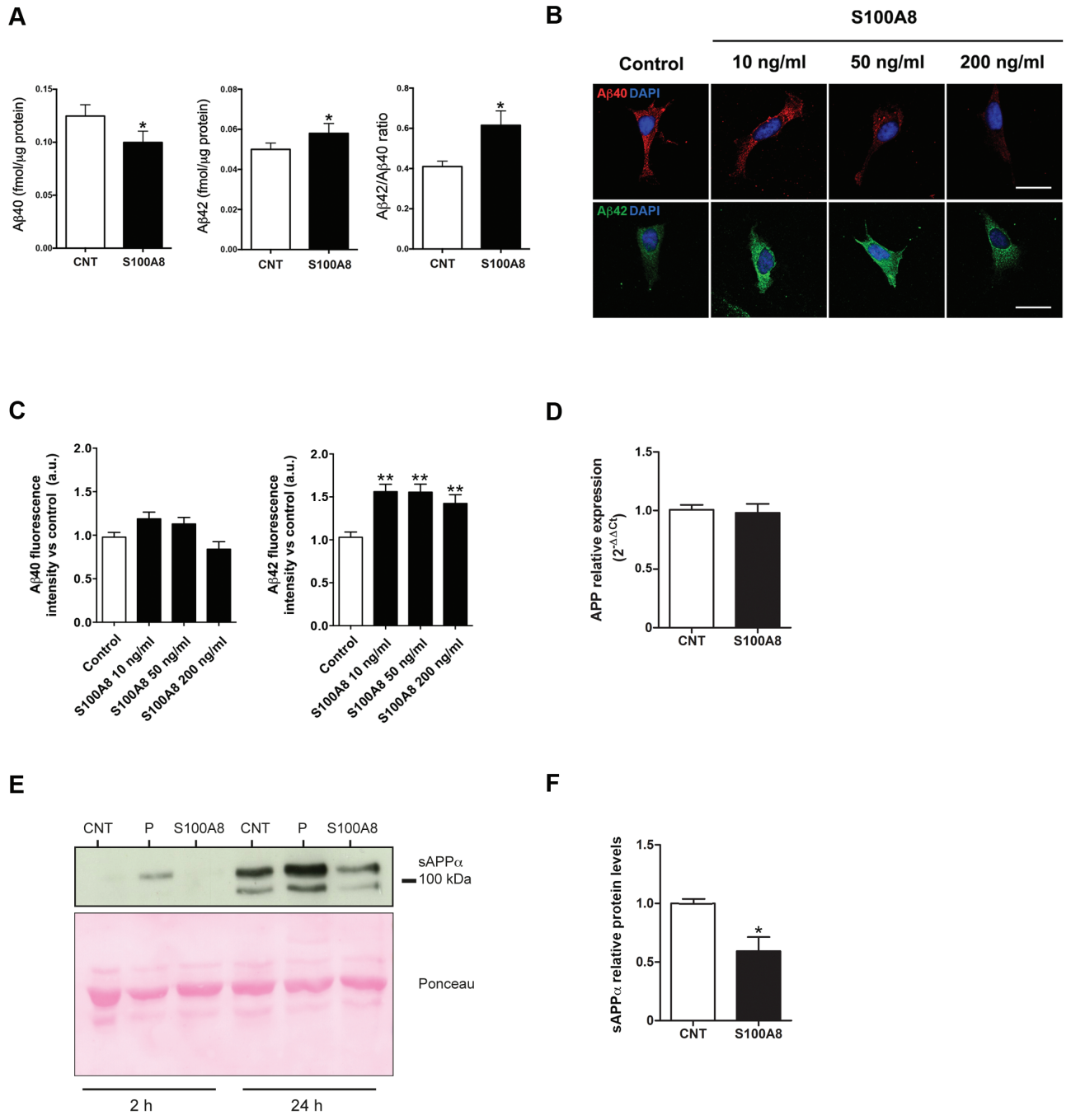

Figure 5. Effects of S100A8 on Aβ production and APP processing in SH-SY5Y cells. (**A**) Enzyme-linked immunosorbent assay measurements of $Aβ_{40}$ (left) and $Aβ_{42}$ (middle) in SH-SY5Y cells treated with S100A8 (200 ng/mL; 24 hours); the $Aβ_{42}/Aβ_{40}$ ratio is shown in the right panel. *$p < .05$; Mann–Whitney *U* test ($n = 6$). (**B**) Confocal microscopy images of SH-SY5Y cells treated with the recombinant S100A8 protein (10, 50 and 200 ng/mL; 24 hours) and immunostained with anti-$Aβ_{40}$ or anti-$Aβ_{42}$ antibodies. (**C**) Quantification of $Aβ_{40}$ and $Aβ_{42}$ immunofluorescences (from 5B). Data were related to control (untreated data), taken as arbitrary units (a.u). Histograms show means ± *SEM* from individual cell fluorescence intensity measures. **$p < .01$; $n = 5$ with a minimum of 10 cells measured per image and condition. (**D**) APP mRNA levels in SH-SY5Y cells treated with recombinant S100A8 protein (200 ng/mL; 24 hours). (**E**) Immunoblotting for sAPPα of conditioned media from SH-SY5Y cells after the following treatments: untreated (CNT), phorbol myristate acetate (50 ng/mL), and S100A8 (200 ng/mL; 24 hours). Ponceau staining is shown as loading control. (**F**) Histogram shows sAPPα data expressed as optical density units and presented as means ± *SEM*. *$p < .05$; $n = 4$; Mann–Whitney *U* test.

Other S100 family proteins such as S100A9 and S100A12 were closely associated with amyloid plaques and neurofibrillary tangles in brains of sporadic and familiar AD cases (47). Moreover, S100B overexpression in mice correlates with AD-related changes such as dystrophic neurite formation, neuronal toxicity, and learning and memory deficits (48). Reduction in S100A9 gene expression results in less amyloid plaques and slower cognitive decline in Tg2576 mice (49,50). S100A9 and S100A8 can form heterodimers, which can self-assemble and oligomerize into amyloid complexes and highly stable fibrils in the aging prostate, highlighting the relationship between inflammation and amyloid deposition (46). S100A8 and S100A9 expressions have been shown to be upregulated after

cytokine stimulation with IL-6 or TNFα in human THF-1 cells (51) and in human prostate cancer (52). The reason for an accelerated S100A8 aggregation in TgAPP mice remains unknown, as well as the impact of S100A8 aggregates on brain pathology. Because S100A8 aggregates were deposited in the hippocampus, a region important for learning and memory, negative consequences for hippocampal function can be suggested. In fact, S100A8 has been shown to activate MAP kinase and NF-kappaB signaling pathways (52), and these were shown to mediate the toxic and proinflammatory effects of Aβ in vitro and in vivo (53,54).

A previous report showed that S100A8 expression can be induced approximately 30-fold in cultured human microglia by chronic treatment with oligomeric Aβ (55). We report that compared with TgAPParc, Tg2576 mice present higher S100A8 accumulation (approximately twofold) and Aβ levels (approximately six- to ninefold). We also performed in vitro studies and corroborated that $A\beta_{42}$ enhances S100A8 production in astrocytes. Thus, a positive correlation between Aβ and S100A8 production could be suggested. However, in an apparent contradiction with this finding, TgAPParc mice showed a threefold increase in S100A8 mRNA levels. It is puzzling to interpret such results, however, it is well known that Aβ and AD pathology also result in altered protein translation (56). Thus, additional Aβ (dose dependent)-induced changes in S100A8 mRNA translation to protein could be suggested.

Moreover, we also demonstrated that S100A8 treatment resulted in strong intracellular accumulation of $A\beta_{42}$ and in decreased levels of extracellular sAPPα products, but not in altered APP expression. Interestingly, S100A8 also induced a parallel decrease in $A\beta_{40}$, which suggests effects on the γ-secretase cleavage of APP, shifting it toward an increased $A\beta_{42}/A\beta_{40}$ ratio. Together, these results support the hypothesis that S100A8 changes APP processing toward increased β-secretase activity and the production of long, more amyloidogenic, Aβ peptides.

A link between S100A8 and Aβ was previously described, as S100A8 is one of the ligands of RAGE and RAGE is the receptor mediating the influx of Aβ into the brain across the blood–brain barrier and its accumulation (21). Several studies support the hypothesis that RAGE expression may be an important contributor and accelerator of neuronal stress, being relevant to AD (57,58). In our paradigm, RAGE expression was not altered in vitro by either S100A8 or $A\beta_{42}$ treatments. In addition, we found S100A8, at a concentration that resulted in an increased $A\beta_{42}$, though not toxic for SH-SY5Y cells. Nevertheless, we can not rule out the possibility that chronic increased S100A8 levels could be deleterious for neurons, either as a result of its mediated Aβ overproduction or RAGE overstimulation. In fact, chronic RAGE stimulation was shown to promote Tau phosphorylation, synaptic dysfunction, and neurodegeneration (59).

Together, our results suggest the existence of a positive feedback between S100A8 and $A\beta_{42}$ generations. In conditions of Aβ overproduction, as in TgAPP animals or FAD mutations, overproduction and hippocampal deposition of S100A8 is likely to occur. Similarly, conditions of chronic brain inflammation (and thus of increased S100A8 production) would result in enhanced $A\beta_{42}$ production by neurons. S100A8 accumulates as extracellular aggregates prior to Aβ plaque formation. S100A8 aggregates increase with aging and do not colocalize with CA or Aβ plaques. Because S100A8 aggregates are abundant in the hippocampus, it is suggested that this could affect learning and memory processes in conditions of aging or Aβ accumulation. Moreover, the possibility that S100A8 aggregates could act as seeds and/or accelerants of brain Aβ deposition could not be ruled out.

Funding

This work was supported by grants from Swedish Brain Power, the regional agreement on medical training and clinical research (ALF) between Stockholm County Council and Karolinska Institutet, Strategic Neuroscience Programme (Sweden), Margaretha af Ugglas Foundation (Sweden), Swedish Alzheimer's Foundation, Swedish Brain Foundation, Foundation Olle Engkvist Byggmästare (Sweden), Gamla Tjänarinnor Foundation (Sweden), Gun och Bertil Stonhes Foundation (Sweden), Blanceflor Boncompagni-Ludovisi Foundation (Italy), Ramon Areces Foundation (Spain), and AFA Soria (Spain). P.M.-S. was supported by an EMBO Long-Term Fellowship (ALTF 696–2013).

References

1. Prince M, Bryce R, Albanese E, Wimo A, Ribeiro W, Ferri CP. The global prevalence of dementia: a systematic review and metaanalysis. *Alzheimers Dement*. 2013;9:63–75.e2. doi:10.1016/j.jalz.2012.11.007
2. Blennow K, de Leon MJ, Zetterberg H. Alzheimer's disease. *Lancet*. 2006;368:387–403. doi:10.1016/S0140-6736(06)69113-7
3. Masters CL, Simms G, Weinman NA, Multhaup G, McDonald BL, Beyreuther K. Amyloid plaque core protein in Alzheimer disease and Down syndrome. *Proc Natl Acad Sci USA*. 1985;82:4245–4249.
4. Goate A, Chartier-Harlin MC, Mullan M, et al. Segregation of a missense mutation in the amyloid precursor protein gene with familial Alzheimer's disease. *Nature*. 1991;349:704–706. doi:10.1038/349704a0
5. Grundke-Iqbal I, Iqbal K, Quinlan M, Tung YC, Zaidi MS, Wisniewski HM. Microtubule-associated protein tau. A component of Alzheimer paired helical filaments. *J Biol Chem*. 1986;261:6084–6089.
6. Heneka MT, Carson MJ, El Khoury J, et al. Neuroinflammation in Alzheimer's disease. *Lancet Neurol*. 2015;14:388–405. doi:10.1016/S1474-4422(15)70016-5
7. Andersen K, Launer LJ, Ott A, Hoes AW, Breteler MM, Hofman A. Do nonsteroidal anti-inflammatory drugs decrease the risk for Alzheimer's disease? The Rotterdam Study. *Neurology*. 1995;45:1441–1445.
8. Stewart WF, Kawas C, Corrada M, Metter EJ. Risk of Alzheimer's disease and duration of NSAID use. *Neurology*. 1997;48:626–632.
9. Côté S, Carmichael PH, Verreault R, Lindsay J, Lefebvre J, Laurin D. Nonsteroidal anti-inflammatory drug use and the risk of cognitive impairment and Alzheimer's disease. *Alzheimers Dement*. 2012;8:219–226. doi:10.1016/j.jalz.2011.03.012
10. Group AR, Martin BK, Szekely C, et al. Cognitive function over time in the Alzheimer's Disease Anti-inflammatory Prevention Trial (ADAPT): results of a randomized, controlled trial of naproxen and celecoxib. *Arch Neurol*. 2008;65:896–905. doi:10.1001/archneur.2008.65.7.nct70006
11. Breitner JC, Haneuse SJ, Walker R, et al. Risk of dementia and AD with prior exposure to NSAIDs in an elderly community-based cohort. *Neurology*. 2009;72:1899–1905. doi:10.1212/WNL.0b013e3181a18691
12. Haass C, Selkoe DJ. Soluble protein oligomers in neurodegeneration: lessons from the Alzheimer's amyloid beta-peptide. *Nat Rev Mol Cell Biol*. 2007;8:101–112. doi:10.1038/nrm2101
13. Abbas N, Bednar I, Mix E, et al. Up-regulation of the inflammatory cytokines IFN-gamma and IL-12 and down-regulation of IL-4 in cerebral cortex regions of APP(SWE) transgenic mice. *J Neuroimmunol*. 2002;126:50–57.
14. McAlpine FE, Lee JK, Harms AS, et al. Inhibition of soluble TNF signaling in a mouse model of Alzheimer's disease prevents pre-plaque amyloid-associated neuropathology. *Neurobiol Dis*. 2009;34:163–177.
15. Ferretti MT, Bruno MA, Ducatenzeiler A, Klein WL, Cuello AC. Intracellular Abeta-oligomers and early inflammation in a model of Alzheimer's disease. *Neurobiol Aging*. 2012;33:1329–1342. doi:10.1016/j.neurobiolaging.2011.01.007
16. Fritz G, Botelho HM, Morozova-Roche LA, Gomes CM. Natural and amyloid self-assembly of S100 proteins: structural basis of functional diversity. *FEBS J*. 2010;277:4578–4590. doi:10.1111/j.1742-4658.2010.07887.x
17. Bucciarelli LG, Wendt T, Rong L, et al. RAGE is a multiligand receptor of the immunoglobulin superfamily: implications for homeostasis and chronic disease. *Cell Mol Life Sci*. 2002;59:1117–1128.

18. Fritz G. RAGE: a single receptor fits multiple ligands. *Trends Biochem Sci*. 2011;36:625–632. doi:10.1016/j.tibs.2011.08.008
19. Park IH, Yeon SI, Youn JH, et al. Expression of a novel secreted splice variant of the receptor for advanced glycation end products (RAGE) in human brain astrocytes and peripheral blood mononuclear cells. *Mol Immunol*. 2004;40:1203–1211.
20. Huttunen HJ, Kuja-Panula J, Sorci G, Agneletti AL, Donato R, Rauvala H. Coregulation of neurite outgrowth and cell survival by amphoterin and S100 proteins through receptor for advanced glycation end products (RAGE) activation. *J Biol Chem*. 2000;275:40096–40105. doi:10.1074/jbc.M006993200
21. Deane R, Du Yan S, Submamaryan RK, et al. RAGE mediates amyloid-beta peptide transport across the blood–brain barrier and accumulation in brain. *Nat Med*. 2003;9:907–913. doi:10.1038/nm890
22. Yan SD, Chen X, Fu J, et al. RAGE and amyloid-beta peptide neurotoxicity in Alzheimer's disease. *Nature*. 1996;382:685–691. doi:10.1038/382685a0
23. Haupt C, Bereza M, Kumar ST, et al. Pattern recognition with a fibril-specific antibody fragment reveals the surface variability of natural amyloid fibrils. *J Mol Biol*. 2011;408:529–540. doi:10.1016/j.jmb.2011.02.032
24. Yan SF, Yan SD, Ramasamy R, Schmidt AM. Tempering the wrath of RAGE: an emerging therapeutic strategy against diabetic complications, neurodegeneration, and inflammation. *Ann Med*. 2009;41:408–422. doi:10.1080/07853890902806576
25. Balducci C, Forloni G. APP transgenic mice: their use and limitations. *Neuromol Med*. 2011;13:117–137. doi:10.1007/s12017-010-8141-7
26. Ronnback A, Zhu S, Dillner K, et al. Progressive neuropathology and cognitive decline in a single Arctic APP transgenic mouse model. *Neurobiol Aging*. 2011;32:280–292. doi:10.1016/j.neurobiolaging.2009.02.021
27. Cedazo-Minguez A, Hamker U, Meske V, et al. Regulation of apolipoprotein E secretion in rat primary hippocampal astrocyte cultures. *Neuroscience*. 2001;105:651–661.
28. Akterin S, Cowburn RF, Miranda-Vizuete A, et al. Involvement of glutaredoxin-1 and thioredoxin-1 in beta-amyloid toxicity and Alzheimer's disease. *Cell Death Differ*. 2006;13:1454–1465. doi:10.1038/sj.cdd.4401818
29. Cedazo-Minguez A, Bonecchi L, Winblad B, et al. Nicergoline stimulates protein kinase C mediated alpha-secretase processing of the amyloid precursor protein in cultured human neuroblastoma SH-SY5Y cells. *Neurochem Int*. 1999;35:307–315.
30. Mateos L, Ismail MA, Gil-Bea FJ, et al. Side chain-oxidized oxysterols regulate the brain renin-angiotensin system through a liver X receptor-dependent mechanism. *J Biol Chem*. 2011;286:25574–25585. doi:10.1074/jbc.M111.236877
31. Zheng L, Calvo-Garrido J, Hallbeck M, et al. Intracellular localization of amyloid-beta peptide in SH-SY5Y neuroblastoma cells. *J Alzheimers Dis*. 2013;37:713–733. doi:10.3233/JAD-122455
32. Ronnback A, Sagelius H, Bergstedt KD, et al. Amyloid neuropathology in the single Arctic APP transgenic model affects interconnected brain regions. *Neurobiol Aging*. 2012;33:831 e811–e839. doi:10.1016/j.neurobiolaging.2011.07.012
33. Gerenu G, Dobarro M, Ramirez MJ, Gil-Bea FJ. Early cognitive stimulation compensates for memory and pathological changes in Tg2576 mice. *Biochim Biophys Acta*. 2013;1832:837–847. doi:10.1016/j.bbadis.2013.02.018
34. Van Paesschen W, Revesz T, Duncan JS. Corpora amylacea in hippocampal sclerosis. *J Neurol Neurosurg Psychiatry*. 1997;63:513–515.
35. Hoyaux D, Decaestecker C, Heizmann CW, et al. S100 proteins in Corpora amylacea from normal human brain. *Brain Res*. 2000;867:280–288.
36. Teigelkamp S, Bhardwaj RS, Roth J, Meinardus-Hager G, Karas M, Sorg C. Calcium-dependent complex assembly of the myeloic differentiation proteins MRP-8 and MRP-14. *J Biol Chem*. 1991;266:13462–13467.
37. Cedazo-Minguez A, Wiehager B, Winblad B, Huttinger M, Cowburn RF. Effects of apolipoprotein E (apoE) isoforms, beta-amyloid (Abeta) and apoE/Abeta complexes on protein kinase C-alpha (PKC-alpha) translocation and amyloid precursor protein (APP) processing in human SH-SY5Y neuroblastoma cells and fibroblasts. *Neurochem Int*. 2001;38:615–625.
38. Walsh DM, Selkoe DJ. Deciphering the molecular basis of memory failure in Alzheimer's disease. *Neuron*. 2004;44:181–193. doi:10.1016/j.neuron.2004.09.010
39. Hardy J, Bogdanovic N, Winblad B, et al. Pathways to Alzheimer's disease. *J Int Med*. 2014;275:296–303. doi:10.1111/joim.12192
40. McGeer PL, McGeer EG, Yasojima K. Alzheimer disease and neuroinflammation. *J Neural Transm Suppl*. 2000;59:53–57.
41. Lue LF, Kuo YM, Beach T, Walker DG. Microglia activation and anti-inflammatory regulation in Alzheimer's disease. *Mol Neurobiol*. 2010;41:115–128. doi:10.1007/s12035-010-8106-8
42. Kummer MP, Vogl T, Axt D, et al. Mrp14 deficiency ameliorates amyloid beta burden by increasing microglial phagocytosis and modulation of amyloid precursor protein processing. *J Neurosci*. 2012;32:17824–17829. doi:10.1523/JNEUROSCI.1504-12.2012
43. Franco R, Cedazo-Minguez A. Successful therapies for Alzheimer's disease: why so many in animal models and none in humans? *Fron Pharmacol*. 2014;5:146. doi:10.3389/fphar.2014.00146
44. Cissé S, Perry G, Lacoste-Royal G, Cabana T, Gauvreau D. Immunochemical identification of ubiquitin and heat-shock proteins in corpora amylacea from normal aged and Alzheimer's disease brains. *Acta Neuropathol*. 1993;85:233–240.
45. Chung MH, Horoupian DS. Corpora amylacea: a marker for mesial temporal sclerosis. *J Neuropathol Exp Neurol*. 1996;55:403–408.
46. Yanamandra K, Alexeyev O, Zamotin V, et al. Amyloid formation by the pro-inflammatory S100A8/A9 proteins in the ageing prostate. *PloS One*. 2009;4:e5562. doi:10.1371/journal.pone.0005562
47. Shepherd CE, Goyette J, Utter V, et al. Inflammatory S100A9 and S100A12 proteins in Alzheimer's disease. *Neurobiol Aging*. 2006;27:1554–1563. doi:10.1016/j.neurobiolaging.2005.09.033
48. Winocur G, Roder J, Lobaugh N. Learning and memory in S100-beta transgenic mice: an analysis of impaired and preserved function. *Neurobiol Learn Mem*. 2001;75:230–243. doi:10.1006/nlme.2000.3961
49. Chang KA, Kim HJ, Suh YH. The role of S100a9 in the pathogenesis of Alzheimer's disease: the therapeutic effects of S100a9 knockdown or knockout. *Neurodegener Dis*. 2012;10:27–29. doi:10.1159/000333781
50. Ha TY, Chang KA, Kim J, et al. S100a9 knockdown decreases the memory impairment and the neuropathology in Tg2576 mice, AD animal model. *PloS One*. 2010;5:e8840. doi:10.1371/journal.pone.0008840
51. Eggers K, Sikora K, Lorenz M, et al. RAGE-dependent regulation of calcium-binding proteins S100A8 and S100A9 in human THP-1. *Exp Clin Endocrinol Diab*. 2011;119:353–357. doi:10.1055/s-0030-1268426
52. Hermani A, De Servi B, Medunjanin S, Tessier PA, Mayer D. S100A8 and S100A9 activate MAP kinase and NF-kappaB signaling pathways and trigger translocation of RAGE in human prostate cancer cells. *Exp Cell Res*. 2006;312:184–197. doi:10.1016/j.yexcr.2005.10.013
53. Lin W, Ding M, Xue J, Leng W. The role of TLR2/JNK/NF-kappaB pathway in amyloid beta peptide-induced inflammatory response in mouse NG108-15 neural cells. *Int Immunopharmacol*. 2013;17:880–884. doi:10.1016/j.intimp.2013.09.016
54. Feld M, Krawczyk MC, Sol Fustinana M, et al. Decrease of ERK/MAPK overactivation in prefrontal cortex reverses early memory deficit in a mouse model of Alzheimer's disease. *J Alzheimers Dis*. 2014;40:69–82. doi:10.3233/JAD-131076
55. Walker DG, Link J, Lue LF, Dalsing-Hernandez JE, Boyes BE. Gene expression changes by amyloid beta peptide-stimulated human postmortem brain microglia identify activation of multiple inflammatory processes. *J Leukoc Biol*. 2006;79:596–610. doi:10.1189/jlb.0705377
56. Bottley A, Kondrashov A. Aberrant translation of proteins implicated in Alzheimer's disease pathology. *OA Genet*. 2013;1:1–5.
57. Fang F, Lue LF, Yan S, et al. RAGE-dependent signaling in microglia contributes to neuroinflammation, Abeta accumulation, and impaired learning/memory in a mouse model of Alzheimer's disease. *FASEB J*. 2010;24:1043–1055. doi:10.1096/fj.09-139634
58. Schmidt AM, Sahagan B, Nelson RB, Selmer J, Rothlein R, Bell JM. The role of RAGE in amyloid-beta peptide-mediated pathology in Alzheimer's disease. *Curr Opin Investig Drugs*. 2009;10:672–680.
59. Li XH, Lv BL, Xie JZ, Liu J, Zhou XW, Wang JZ. AGEs induce Alzheimer-like tau pathology and memory deficit via RAGE-mediated GSK-3 activation. *Neurobiol Aging*. 2012;33:1400–1410. doi:10.1016/j.neurobiolaging.2011.02.003